9-29-2004

On the Grunbaum Commutor Based Discrete Fractional Fourier Transform

Bal Santhanam

Juan Vargas-Rubio

DEPARTMENT OF ELECTRICAL AND COMPUTER ENGINEERING

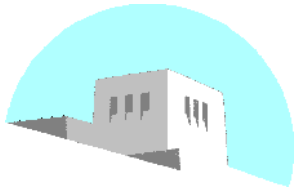

SCHOOL OF ENGINEERING
UNIVERSITY OF NEW MEXICO

On the Grunbaum Commutor Based Discrete Fractional Fourier Transform

Balu Santhanam and Juan. G. Vargas-Rubio
Department of Electrical & Computer Engineering
University of New Mexico, Albuquerque, NM: 87131
Tel: 505 277-1611, Fax: 505 277 1439
Email: bsanthan,jgvargas@eece.unm.edu

UNM Technical Report: EECE-TR-04-22

Report Date: September 29, 2004

Abstract

The basis functions of the *continuous fractional Fourier transform* (FRFT) are linear chirp signals that are suitable for time-frequency analysis of signals with chirping time-frequency content. In the continuous–time case, analytical results linking the chirp rate of the signal to a specific angle where the FRET of the chirp signal is an impulse exist. Recent efforts towards developing a discrete and computable version of the fractional Fourier transform (DFRFT) have focussed on furnishing a orthogonal set of eigenvectors for the DFT that serve as discrete versions of the Gauss–Hermite functions in the hope of replicating this property. In the discrete case, however, no analytical results connecting the chirp rate of the signal to the angle at which we obtain an impulse exist. Defined via the fractional matrix power of the centered version of the DFT, computation of this transform has been constrained due to the need for computing an eigenvalue decomposition. Analysis of the centered version of the DFRFT obtained from Grunbaum's tridiagonal commuter and the kernel associated with it reveals the presence of both amplitude and frequency modulation in contrast to just frequency modulation seen in the continuous case. Furthermore, the instantaneous frequency of the basis functions of the DFRFT are sigmoidal rather than linear. In this report, we define a centered version of the DFRFT based on the Grunbaum commutor and investigate its capabilities towards representing and concentrating chirp signals in a few transform coefficients. We then propose a fast algorithm using the FFT for efficient computation of the multiangle version of the CDFRFT (MA-CDFRFT) using symmetries in the computed eigenvectors to reduce the size of the eigenvalue problem. We further develop approximate empirical relations that will enable us to estimate the chirp rate of the multicomponent chirp signals from the peaks of the computed MA-CDFRFT. This MA-CDFRFT also lays the ground work for a novel chirp rate Vs. frequency signal representation that is more suitable for the time-frequency analysis of multicomponent chirp signals.

Keywords

Discrete fractional Fourier transform, linear chirp signals, chirp rate estimation, discrete Fourier transform, chirp rate/frequency representation.

1 Introduction

The continuous–time Fractional Fourier transform of a signal $x(t)$ is defined via the integral [9]:

$$X_\alpha(t,u) = \mathbf{F}_\alpha(x(t)) = \int_{-\infty}^{\infty} x(t) K_\alpha(t,u) dt,$$

where the Kernel of the transform is given by:

$$K_\alpha(t,u) = \sqrt{\frac{1-j\cot\alpha}{2\pi}} \exp\left(j\frac{t^2+u^2}{2}\cot\alpha - jtu\csc\alpha \right).$$

This integral operator constitutes a involution operator [18] of order 4 on the space of square integrable signals and constitutes a rotation operation in time-frequency space:

$$\mathbf{F}_0 = \mathbf{I}, \;\; \mathbf{F}^4 = \mathbf{I},$$

and the operator $\mathbf{F}$ denotes the conventional Fourier transformation given by:

$$\mathbf{F}(x(t)) = X(\omega) = \frac{1}{\sqrt{2\pi}} \int_{-\infty}^{\infty} x(t) \exp(-j\omega t)\, dt.$$

The kernel of the FRET can be expanded via Mercer's theorem as:

$$K_\alpha(t,u) = \sum_{p=-\infty}^{\infty} e^{-jp\alpha} H_p(t) H_p(u),$$

where $H_p(t)$ corresponds to the k-th order Gauss Hermite function,

$$H_k(t) = \frac{2^{1/4}}{\sqrt{2^k k!}} e^{-\pi t^2} h_k(t),$$

where $h_k(t)$ is the k-th order Hermite polynomial. The FRET basis functions are linear chirp signals which provides a framework for analysis of signals with linear-FM type time-frequency content and is the driving force behind the quest for a discrete fractional Fourier transform. A DFRFT preserving the rotation aspect of the continuous–time FRET was defined via the fractional power of the DFT matrix [8]:

$$\mathbf{A}_\alpha(\mathbf{x}) = \mathbf{W}^{\frac{2\alpha}{\pi}}(\mathbf{x}) = \sum_{p=0}^{N-1} e^{-jp\alpha} \mathbf{v}_p \mathbf{v}_p^H(\mathbf{x}). \tag{1}$$

Properties of this DFRFT were analyzed in [8], where it was shown to be a rotation in discrete time–frequency space. Specifically using a Taylor series expansion of the fractional power, the discrete fractional Fourier transform operator can be expanded as:

$$\mathbf{A}_\alpha = a_0(\alpha)\mathbf{I} + a_1(\alpha)\mathbf{W} + a_2(\alpha)\mathbf{W}^2 + a_3(\alpha)\mathbf{W}^3, \tag{2}$$

where the coefficients $a_i(\alpha), i = 0,1,2,3$ are constants defined in [8]. The expansion in [8], however, is based on eigenvectors of the DFT that are linearly independent but non orthogonal set. Specifically the DFT has 4 distinct eigenvalues and only those that belong to distinct eigenvalues are orthogonal. Since the basis functions of the continuous FRET are not bandlimited, directly sampling of the kernel will result in aliasing and approaches based on oversampling will result in a non orthogonal basis [13, 15]. Other approaches such as the chirp Fourier transform that directly use discrete–time chirp functions in the kernel have also been proposed but here again the basis functions are not orthogonal [15]. Earlier work in [1] furnishes an expression for orthogonal DFT eigenvectors based on sampling and aliasing of the Gauss–Hermite functions but does not yield a computable version. Recent efforts towards finding a discrete FRET have focussed on the problem of furnishing orthogonal

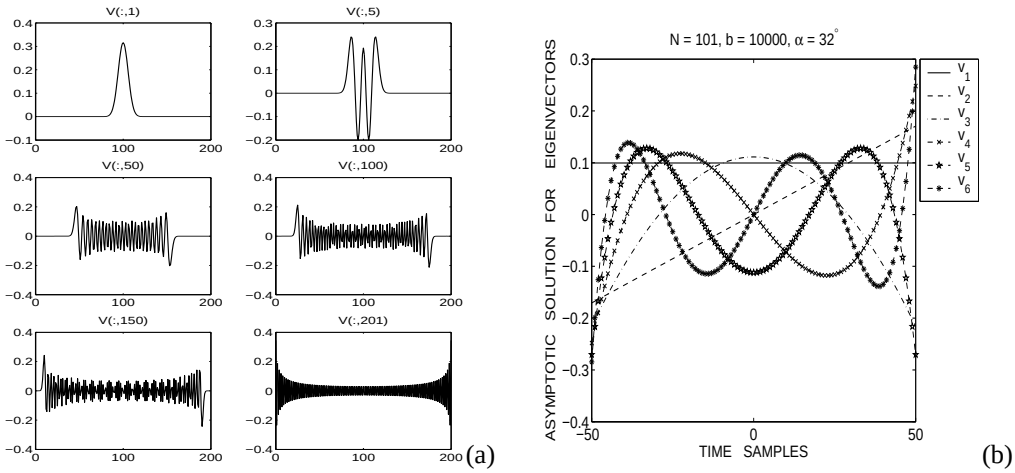

Figure 1: Eigenvectors of the Grunbaum tridiagonal commuting matrix $\mathbf{T}$ for $N = 201, \alpha = 22.5^\circ, b = 1$. Note that the k^{th} eigenvector has $k-1$ zero crossings, (b) asymptotic solution for the eigenvectors $v_k[n], k = 1,2,3,4,5,6$.

eigenvectors for the DFT, that are discrete versions of the Hermite–Gauss functions. One of these approaches based on the work by Dickinson and Steiglitz and the Harper matrix **S** has been used for constructing a complete orthogonal set of eigenvectors for DFT eigenvectors [4, 16].

$$v[n+1] - 2v[n] + v[n-1] + 2\left(\cos\left(\frac{2\pi}{N}n\right) - 1\right)v[n] = \lambda v[n].$$

For N that is a multiple of 4, the Harper matrix has a single zero eigenvalue and the problems associated with this were resolved in [16]. Another discrete version of the FRET based on Kravchuk functions has been explored in [2].

$$\Phi_n[m] = \frac{1}{2^{l-m}}\sqrt{\binom{2l}{l+m}/\binom{2l}{n}}\,k_n(l+m,2l),$$

where $k_n(r,2s) = \frac{(-1)^n}{2^n}{}_2F_1(-n,-r;-2s;2)$ is the symmetric Kravchuk polynomial.

The particular approach towards obtaining the DFT eigenvectors adopted in this report uses the tridiagonal commuting matrix introduced by Grunbaum [14]. The motivation behind using this particular approach is that:

1. it furnishes a complete basis for the DFT for any N. This is not the case for approaches based on the Harper matrix where a degeneracy still exists when N is a multiple of 4.

2. the Grunbaum tridiagonal commuting matrix in the limit approaches the second-order differential Hermite-Gauss operator [14].

3. the Grunbaum eigenvectors are better approximations to the continuous Gauss–Hermite functions than the eigenvectors obtained through the Harper matrix approach.

Recently Mugler and Clary modified the Grunbaum tridiagonal incorporating a scaling factor and the resultant eigenvectors very closely resemble the Gauss-Hermite functions [11]. In this report, we will focus our analysis on the latter and analyze the discrete FRET obtained from this commutor, study the properties of the transform and the associated basis functions. Specifically we will see that the basis functions contain both amplitude and frequency modulation to preserve orthogonality.

2 On the Grunbaum DFRFT

The motivation behind the commutor matrix approach towards finding the DFT eigenvectors lies in the fact that if two unitary–symmetric matrices **A** and **B** commute then they share a basis of eigenvectors. If the eigenvalues of the commuting matrix **B** are distinct the eigenvectors of the commutor without degeneracy furnish the sought eigenvectors. The tridiagonal commutor of Grunbaum is defined via its diagonal, off-diagonal elements [11]

$$\mathbf{T}_{mn} = \begin{cases} -2\cos(\pi N\tau)\sin(\pi n\tau)\sin(\pi(N-n-1)\tau) \\ \text{if } \ m=n, \ \ 0 \le n \le N-1, \\ \sin(\pi n\tau)\sin(\pi(N-n)\tau) \\ \text{if } \ m=n+1, n-1, \ \ 1 \le n \le N-1, \\ 0, \ \ \text{otherwise} \end{cases}$$

where $0 \le \mu \le N-1$ and $\tau = 1/Nb^2$. Next we focus our attention on the centered version of the DFT matrix operator defined via [11]:

$$\{\mathbf{W}_{a,b}\}_{mn} = \frac{1}{\sqrt{N}} \exp\left(-j\frac{2\pi}{N}(m-a)(n-a)/b^2\right),$$

where the shift parameter $a = \frac{N-1}{2}$. Note that this corresponds to a shifted version of the DFRFT only when N is odd. This focus is due to the fact that the eigenvalues of the commutor matrix **T** for the centered DFRFT case are both real and unique and furnish the complete orthogonal set of DFT eigenvectors $\mathbf{V}_G$ via [11]: $\mathbf{T} = \mathbf{V}_G \Lambda_G \mathbf{V}_G^T$. It is also instructive to look at some specific observations regarding the DFRFT that arise out of this expansion in Eq. (1). First, the DFRFT matrix operator is an involution operator of order $m = \text{floor}(\frac{2\pi}{\alpha})$: $\mathbf{A}_\alpha^m = \mathbf{I}$. Specifically when $\alpha = \frac{\pi}{2}$ it reduces to the DFT matrix which is $m = 4$-th order involution. The involution property is derived from the eigenvalues of the DFRFT operator and is independent of the eigenvectors. It is also an indicator of the fact that this operator represents a rotation in time–frequency space. The eigenvalues of the DFRFT matrix operator are the roots of unity and when the angle α takes on discrete values $\alpha = \frac{2\pi}{N}p, p = 0, 1, \ldots, N-1$, the trace of the operator vanishes at the zeroes of the Dirichlet kernel:

$$\text{Trace}(\mathbf{A}_\alpha) = D_N(\alpha) = e^{-j\alpha(N-1)/2}\left(\frac{\sin(N\alpha/2)}{\sin(\alpha/2)}\right). \tag{3}$$

When the trace of the DFRFT is actually zero, i.e., $\alpha = \alpha_r = \frac{2\pi r}{N}$ the determinant of the DFRFT operator becomes:

$$\det(\mathbf{A}_\alpha) = \prod_{p=1}^{N} \exp(-jp\alpha_r) = \pm 1, \ \ \alpha_r = \frac{2\pi r}{N} \tag{4}$$

This fact is important from the perspective of development of fast algorithms for computing the DFRFT because the DFRFT can now be interpreted as a DFT:

$$\mathbf{A}_r(\mathbf{x}) = \sum_{p=0}^{N-1} \mathbf{v}_p \mathbf{v}_p^H(\mathbf{x}) \exp\left(-j\frac{2\pi}{N}rp\right).$$

Specifically on an element by element basis the DFRFT reduces to:

$$X_r[k] = \sum_{p=0}^{N-1} \left\{ v_{kp} \sum_{n=0}^{N-1} v_{np} x[n] \right\} W_N^{pr}, \tag{5}$$

where v_{ij} refers to the (i,j)-th element of the matrix of eigenvectors $\mathbf{V}_G$ of the Grunbaum tridiagonal commutor. This relation specifies the DFRFT as an angular DFT that which can be computed using the computationally efficient FFT algorithm. Since the Grunbaum commutor matrix is real, symmetric and tridiagonal methods such as the Lancoz algorithm [20] can be used to compute the eigenvectors needed for the DFT. The four term power

series expansion of [8] is not valid for the DFRFT based on the Grunbaum commutor. However, the DFRFT operator can still be expanded as a power series of the form:

$$\mathbf{A}_\alpha = \sum_{i=0}^{N-1} a_i(\alpha) \left[\log(\mathbf{W})\right]^i.$$

The eigenvectors of the Grunbaum tridiagonal commutor $v_k^{(b)}[n]$ for $N = 201, b = 1, \alpha = 22.5^\circ$ are described in Fig. (1)(a). Note that the eigenvector of order k exhibits $k-1$ zero crossings as in the case of the continuous Gauss-Hermite functions. The effect of the dilation parameter on the eigenvectors of $\mathbf{T}$ is illustrated in Fig. (1)(b) for different values of the dilation parameter b. Note that the dilation parameter only affects the eigenvectors and not the eigenvalues of the DFRFT. As the dilation parameter value increases, the spread of the eigenvector $v_1[n]$ increases. Furthermore negative values of dilation parameter b produce the same results as the corresponding positive dilation parameter, i.e., $v_k^{(b)}[n] = v_k^{(-b)}[n]$, indicating a dependence on just $|b|$. These eigenvectors $v_k^{(b)}[n]$ exhibit even or odd symmetry: $v_k^{(b)}[n] = \pm v_k^{(b)}[-n]$ depending on the order k requiring the storage of just half of the N samples for each eigenvector. It has been shown by Grunbaum [14] that the tridiagonal commutor matrix $\mathbf{T}$ commutes with the centered version of the DFT. The eigenvectors of the Grunbaum tridiagonal commutor in particular satisfy a second order difference equation of the form:

$$\begin{aligned} v_k[1] &= \frac{\lambda_k - a_0}{b_1} v_k[0] \\ b_{n+1} v_k^{(b)}[n] + (a_{n+2} - \lambda_k) v_k^{(b)}[n+1] &+ b_{n+2} v_k^{(b)}[n+2] = 0, \end{aligned}$$

where $a_n = \mathbf{T}_{nn}, \quad 0 \le n \le N-1$ and $b_n = \mathbf{T}_{n,n-1}, \quad 1 \le n \le N-1$. Fig. (1)(b) describes the effect of a very large dilation parameter b on the eigenvectors $v_2[n], v_3[n]$ and $v_4[n]$ of the Grunbaum tridiagonal commutor $\mathbf{T}$. An important observation that one derives from Fig. (1)(b) is that in the limit of a large dilation parameter the solution to this second-order difference equation $v_k^{(b)}[n]$ approaches a polynomial similar to the way in which the Hermite Gauss functions asymptotically tend to Hermite polynomials:

$$v_k^{(b)}[n] = p_k[n] \psi_k^{(b)}[n], \quad \lim_{b \to \infty} \psi_k^{(b)}[n] = 1. \tag{6}$$

3 Analysis of the Grunbaum DFRFT

Specifically the kernel of the DFRFT based on the Grunbaum tridiagonal commutor contains both amplitude modulation and frequency modulation in an effort to preserve orthogonality:

$$K_\alpha[n,k] = A_\alpha[n,k] \exp\left(j \Phi_\alpha[n,k]\right), \tag{7}$$

where $A_\alpha[n,k]$ is the instantaneous envelope of the kernel and $\Phi_\alpha[n,k]$ is the instantaneous phase of the kernel. As a consequence of this information the DFRFT can be interpreted as an AM–FM transform of the form:

$$X_\alpha[k] = \sum_{n=0}^{N-1} A_\alpha[n,k] \exp\left(j \Phi_\alpha[n,k]\right) x[n] \tag{8}$$

The AM and FM modulation parts in particular satisfy:

$$\begin{aligned} \lim_{\alpha \to 90^\circ} A_\alpha[n,k] &= \frac{1}{\sqrt{N}}, \ \lim_{\alpha \to 90^\circ} \Phi_\alpha[n,k] = \frac{2\pi n k}{N} \\ \lim_{\alpha \to 0^\circ} A_\alpha[n,k] &= \delta[n-k]. \end{aligned}$$

Fig. (4)(a) describes the instantaneous envelope of the DFRFT kernel for $\alpha = 22.5^\circ, b = 1, N = 201$. Fig. (4)(b) describes the instantaneous envelope of a specific column of the DFRFT matrix for different angular parameters describing the increasing spread of the envelope from a impulse to a constant. Fig. (2) describes the instantaneous frequency of the columns of the DFRFT where we note that Fig. (3) describes the instantaneous unwrapped phase associated with the kernel of the DFRFT for $N = 101, b = 1$. the IF of the kernel is not linear as in the case of the continuous FRET kernel but rather sigmoidal. Also note that as the angular parameter α approaches 90° the IF starts to approach a constant corresponding to the sinusoidal basis functions of the DFT kernel.

4 Grunbaum DFRFT : $N = 2$ case

In general the DFRFT matrix operator is defined via the fractional matrix power of the DFT matrix:

$$\mathbf{A}_\alpha = \mathbf{V}_c \Lambda^{\frac{2\alpha}{\pi}} \mathbf{V}_c^T,$$

where $\mathbf{V}_c$ is the matrix eigenvectors obtained from Grunbaum's tridiagonal commutor matrix $\mathbf{T}$. The DFRFT operator for the case where $N = 2$ is given by:

$$\mathbf{A}_\alpha = \frac{1}{\sqrt{2}} \begin{pmatrix} 1 & 1 \\ 1 & -1 \end{pmatrix} \begin{pmatrix} 1 & 0 \\ 0 & e^{-j\alpha} \end{pmatrix} \frac{1}{\sqrt{2}} \begin{pmatrix} 1 & 1 \\ 1 & -1 \end{pmatrix}^T$$

Simplifying this expression yields:

$$\mathbf{A}_\alpha = e^{-j\frac{\alpha}{2}} \underbrace{\begin{pmatrix} \cos\frac{\alpha}{2} & j\sin\frac{\alpha}{2} \\ j\sin\frac{\alpha}{2} & \cos\frac{\alpha}{2} \end{pmatrix}}_{\mathbf{M}}$$

Note that in this specific case, the matrix of eigenvectors is also identical to the DFT matrix operator of dimension $N = 2$, i.e., $\mathbf{W}_2$, and consequently:

$$\mathbf{A}_\alpha = \mathbf{W}_2 \begin{pmatrix} 1 & 0 \\ 0 & e^{-j\alpha} \end{pmatrix} \mathbf{W}_2.$$

Multiplication by the diagonal matrix corresponds to twiddle factor multiplication in between the two DFT operations. However, the matrix of eigenvectors V_c is not in general a symmetric matrix. A second interesting observation is that the matrix $\mathbf{M}$ is the complex equivalent of the 2×2 rotation matrix that is given by:

$$\mathbf{R}_\theta = \begin{pmatrix} \cos\theta & -\sin\theta \\ \sin\theta & \cos\theta \end{pmatrix},$$

with the observation that the -1 along the off-diagonals of $\mathbf{R}_\theta$ has been distributed as $j \times j$ along the off-diagonal of $\mathbf{M}$.

5 Grunbaum DFRFT: $N = 3$ case

For the case where $N = 3$, however, the matrix of eigenvector $\mathbf{V}_c$ is more complex:

$$\mathbf{V}_c = \begin{pmatrix} \frac{1}{\sqrt{6+2\sqrt{3}}} & \frac{-1}{\sqrt{2}} & \frac{1}{\sqrt{6-2\sqrt{3}}} \\ \frac{\sqrt{3}+1}{\sqrt{6+2\sqrt{3}}} & 0 & -\frac{\sqrt{3}-1}{\sqrt{6-2\sqrt{3}}} \\ \frac{1}{\sqrt{6+2\sqrt{3}}} & \frac{1}{\sqrt{2}} & \frac{1}{\sqrt{6-2\sqrt{3}}} \end{pmatrix}$$

Note that in this case the matrix of eigenvectors $\mathbf{V}_c$ is not symmetric and is not the same as the DFT matrix $\mathbf{W}_3$. The DFRFT matrix operator in this case then becomes:

$$\mathbf{A}_\alpha = \mathbf{V}_c \begin{pmatrix} 1 & 0 & 0 \\ 0 & e^{-j\alpha} & 0 \\ 0 & 0 & e^{-j2\alpha} \end{pmatrix} \mathbf{V}_c^T.$$

Upon simplification this yields the expression:

$$\mathbf{A}_\alpha = \frac{1}{2} e^{-j\alpha} \begin{pmatrix} 1+\cos\alpha - \frac{j}{\sqrt{3}}\sin\alpha & \frac{2j}{\sqrt{3}}\sin\alpha & \cos\alpha - 1 - \frac{j}{\sqrt{3}}\sin\alpha \\ \frac{2j}{\sqrt{3}}\sin\alpha & 2\cos\alpha + \frac{2j}{\sqrt{3}}\sin\alpha & \frac{2j}{\sqrt{3}}\sin\alpha \\ \cos\alpha - 1 - \frac{j}{\sqrt{3}}\sin\alpha & \frac{2j}{\sqrt{3}}\sin\alpha & \cos\alpha + 1 - \frac{j}{\sqrt{3}}\sin\alpha \end{pmatrix}$$

6 Generalization from the $N = 2$ case

We can generate a generalization of the DFRFT for the general case from the case where $N = 2$ via:

$$\tilde{\mathbf{A}}_\alpha = \mathbf{W}_N \Lambda^{\frac{2\alpha}{\pi}} \mathbf{W}_N^H$$

This corresponds to a transform of the form:

$$X_\alpha[k] = \frac{1}{N} \sum_{n=0}^{N-1} \sum_{p=0}^{N-1} x[n] \exp\left(-j\frac{2\pi}{N}\left(n-k+\frac{N\alpha}{2\pi}\right)p\right) = x\left[\left(\left(k-\frac{N\alpha}{2\pi}\right)\right)_N\right].$$

Ofcourse intuitively this corresponds to just a phase modification in the DFT of the signal $x[n]$.

7 The Multi–Angle CDFRFT Representation

Using the definition of the CDFRFT, we now develop a fast algorithm for computing the multiple angle version of the CDFRFT. The elements of the CDFRFT matrix can be expressed as

$$\{\mathbf{A}_\alpha\}_{kn} = \sum_{p=0}^{N-1} v_{kp} v_{np} e^{-jp\alpha}, \tag{9}$$

where v_{kp} is the k-th element of p-th eigenvector . Multiplying $\mathbf{A}_\alpha$ by the signal $x[n]$ we obtain the transform:

$$X_\alpha[k] = \sum_{n=0}^{N-1} x[n] \sum_{p=0}^{N-1} v_{kp} v_{np} e^{-jp\alpha}, \tag{10}$$

and after rearranging the two sums we obtain:

$$X_\alpha[k] = \sum_{p=0}^{N-1} v_{kp} \sum_{n=0}^{N-1} x[n] v_{np} e^{-jp\alpha}. \tag{11}$$

If we use a discrete set of angles given by

$$\alpha = \alpha_r = \frac{2\pi r}{N}, \;\; r = 0, 1, \ldots, N-1, \tag{12}$$

we obtain

$$X_r[k] = \sum_{p=0}^{N-1} v_{kp} \sum_{n=0}^{N-1} x[n] v_{np} e^{-j\frac{2\pi}{N}pr}. \tag{13}$$

Defining $z_k[p]$ as

$$z_k[p] = v_{kp} \sum_{n=0}^{N-1} x[n] v_{np}, \tag{14}$$

we observe that the transform can be expressed as the DFT of $z_k[p]$, that is

$$X_k[r] = \sum_{p=0}^{N-1} z_k[p] W_N^{pr},\ 0 \leq r,k \leq N-1. \tag{15}$$

Expressing the transform as a DFT allows us to use the regular FFT algorithm for computing the CDFRFT. The resulting transform $X_k[r]$ containing the CDFRFT for these discrete angles is called the *multi–angle* DFRFT (MA-DFRFT).

Further simplifications in the algorithm are obtained by:

1. incorporating the even and odd symmetries of the Grunbaum eigenvectors to reduce the number of multiplications needed [19].
2. exploiting the observation that a lot of the entries in the matrix of eigenvectors are very close to zero and can effectively be approximated by zero thereby reducing the number of multiplications required even further without introducing significant error [19].
3. Exploiting symmetries in the signal under analysis so that the MA-CDFRFT for a certain number of angles are needed.

The MA-CDFRFT is a matrix, $\mathbf{X}_k[r]$, that contains a representation of the signal in which time and frequency share the same axis (index k), and depending on the value of α we interpret the index as time or frequency. There is a diamond shaped region in the space $\mathbf{c_r}$–ω_0 where for a signal with constant chirp rate we have a good localization of the chirp rate and the average frequency of a signal, and where index k is interpreted as frequency [19]. Figure 9 shows a representation of the matrix that indicates where the region is located in matrix $\mathbf{X}_k[r]$. When we compute the MA-CDFRFT of a complex sinusoidal signal we obtain always two peaks, one in the lower half and other in the upper half of $\mathbf{X}_k[r]$, and if the signal has a constant frequency, the peaks will be located exactly at the rows corresponding to angles α=90 and α=270 that correspond to the centered DFT (CDFT), and its inverse respectively. With a real signal we obtain four peaks due to the fact that it has negative and positive frequencies. A signal with a chirp rate different than zero will produce peaks at angles different than 90 and 270, and they will be above or below those values depending on the sign of the chirp rate.

8 Relating Chirp Rate & Angle

The approach used here is to find the chirp rate of the signal that results in the largest peak in the magnitude of the MA-DFRFT for a the discrete set of angles defined before. We first look at complex chirps with zero average frequency of the form

$$x[n] = e^{j\mathbf{c_r}(n-\frac{N-1}{2})^2},\ 0 \leq n \leq N-1,$$

where $\mathbf{c_r}$ is the chirp rate. After performing the computation for different sizes transform sizes, the results show that the relation between the chirp rate $\mathbf{c_r}$ and angle α can be described approximately by the relation

$$\mathbf{c_r} = \pi \frac{\tan(\alpha - \pi/2)}{N}. \tag{16}$$

This relation is not exact and has an error slightly larger than 10% for some angles. A plot of the results for $N = 128$ is given in Fig. 8.

The other aspect of this approximation that we wish to determine is how good the concentration of the chirp function for the values obtained before is. For this purpose we computed the number of coefficients of the transformed signal that captured 50% of the total energy. The result of this computation reveals that we only get good concentration of the chirp signal in the interval of angles from 45 to 135, and in this range, 50% of the energy is concentrated in at most two coefficients. Outside the interval the number of coefficients grows rapidly, as it can be seen in Fig. 10(a).

Let us now consider the case of chirp signals having an average frequency different than zero, i.e.,

$$x[n] = e^{j(\mathbf{c_r}(n-(N-1)/2)^2+\omega_0(n-(N-1)/2))}, \;\; 0 \leq n \leq N-1.$$

where ω_0 is the average frequency. The other point of interest is where the maximum concentration occurs and is a measure of how well the CDFRFT can localize the average frequency of this chirp signal. In addition to the computation of the chirp rate and the number of coefficients needed for capturing 50% of the energy, we also compute the coefficient at which the maximum value occurs. The results show little difference in the relation of the chirp rate with the angle α compared with the case of zero average frequency. The number of coefficients that concentrate 50% of the energy of the signal is also similar to the zero average frequency case, but as the average frequency increases, the interval for which we concentrate the signal in two coefficients decreases slightly. Fig. 10(b) shows the case for $\omega_0 = 1.57$. The error in the localization of the average frequency, measured as the difference between the coefficient of the average frequency and the coefficient at which the peak occurs, shows that as the average frequency increases, the error also increases. Fig. 10(c) shows this difference for positive frequencies. The larger deviations correspond to larger frequencies. This result is also affected by aliasing and consequently we ignore combination of large chirp rate and large average frequency.

From the results in previous sections, we see that for alpha between 45 to 135 we obtain better concentration of signal energy when analyzing linear chirps. For this interval, we have found empirically that the relation between the angle of the transform and the chirp rate can be approximated better if we add a linear term to Eq.(16) and the corresponding error is reduced to less than 2% :

$$\mathbf{c_r} = 2\frac{\tan(\alpha-\pi/2)}{N} + 1.41\frac{(\alpha-\pi/2)}{N}. \tag{17}$$

This relation is useful for determining the chirp rate from the angle at which we have more concentration, particularly when we the MA-CDFRFT algorithm described before is used.

9 Examples: Chirp Rate Estimation

Our goal in this section, is to study the utility of the two approximate expressions relating the chirp rate to the transform angle. The first example pertains to the application of the MA-DFRFT to a single linear chirp signal:

$$x[n] = e^{j(\mathbf{0.005}(n-\frac{127}{2})^2)}, \;\; 0 \leq n \leq 127$$

Fig. 11(a) shows the complex chirp signal, Fig. 11(b) describes the magnitude of the MA-DFRFT of this signal. Specifically we observe that we actually have two maxima because the CDFRFT at $\alpha+\pi$ is reversed version of the CDFRFT at α. The location of the maximum is at $r = 36$ which corresponds to an angle $\alpha = 2\pi\frac{36}{128} = 1.7671$. Upon application of Eq. (16) the corresponding chirp rate estimate is 0.0049, while application of Eq. (17) yields a chirp rate of 0.0053. Fig. 11(c) is the slice of the MA-DFRFT at this particular angle, where the magnitude of the MA-DFRFT is a maximum.

Adding another chirp component with zero average frequency at a different chirp rate yields a two-component chirp signal. The MA-DFRFT and the approximate relations are applied to estimate the two chirp rates associated with the two-component chirp signal. The second chirp component has a negative chirp rate of 0.007. For this case the maxima occur at $r = 36$ and $r = 27$ and the corresponding chirp rates from application of Eq. (16) are

0.0049 and -0.0062. The corresponding chirp rates obtained via Eq. (17) are 0.0053 and -0.0066. The chirp signal, its MA-DFRFT and its slice at the angle where the magnitude of the MA-DFRFT is a maximum are shown in Fig. (11). In both cases, we can see that the MA-DFRFT is able to concentrate chirp signals into a few coefficients and that Eq. (16) and Eq. (17) can be used to estimate the chirp rate(s) of the signal.

10 Conclusion

In this report, we have studied the capability of the centered DFRFT obtained from the Grnbaum commuting matrix to concentrate a chirp signal in a few transform coefficients. We presented an FFT based algorithm for computing the multi-angle version of the CDFRFT. We then furnished two empirical relations that related the chirp rate and the angle that produced a impulse-like transform. We evaluated the efficacy of these expressions by applying these relations to the analysis of single and two component chirps signals and demonstrated that the CDFRFT and its multi-angle version are powerful time-frequency tools for the analysis of both monocomponent and multicomponent chirp signals.

References

[1] M. L. Mehta, "Eigenvalues and Eigenvectors of the finite Fourier Transform," *Journal of Mathematical Physics*, Vol. 28, No. 4, 1987.

[2] N. M. Atakishiev and K. B. Wolf, "Fractional Fourier–Kravchuk Transform," *Journal Opt. Soc. of Amer.*, Vol. 14, No. 7, pp. 1467-1477, 1997.

[3] N. M. Atakishiev, L. E. Vicent and K. B. Wolf, "Continuous vs. discrete fractional Fourier Transforms," *Journal of Computational and Applied Mathematics* Vol. 107, pp. 73-95, 1999.

[4] B. W. Dickinson and K. Steiglitz, "Eigenvalues and Eigenvectors of the Discrete Fourier Transform," *IEEE Trans. ASSP*, Vol. 30, No. 1, Feb 1982.

[5] G. Strang, "Linear Algebra and Its Applications," New York, Academic Press, 1976.

[6] T. S. Santhanam, "An Algorithm for the Basis of the Finite Fourier Transform," *Second International Workshop on Harmonic Oscillators*, pp. 239-248, Cocoyoc, Mexico, 1994.

[7] Balu Santhanam and J. H. McClellan, "The DRFT: A Rotation in Time–Frequency Space," *Proceedings of ICASSP-95*, Vol. 2, pp. 921-924, May 1995.

[8] B. Santhanam and J. H. McClellan, "The Discrete Rotational Fourier Transform," *IEEE Trans. Sig. Process.*, Vol. 44, No. 4, pp. 994-998, 1996.

[9] L. B. Almeida, "The Fractional Fourier Transform and Time–Frequency Representations," *IEEE Trans. Sig. Process.*, Vol. 42, No. 11, pp. 3084-3091, 1994.

[10] D. H. Mugler, S. Clary, Y. Wu, "Discrete Hermite Expansion of Digital Signals: Applications to ECG Signals," *Proceedings of IEEE DSP Workshop*, Pine Mountains, Georgia, Oct 2002.

[11] S. Clary and D. H. Mugler, "Shifted Fourier Matrices and Their Tridiagonal Commutors," *SIAM Jour. Matr. Anal. & Appl.*, Vol. 24, No. 3, pp. 809-821, 2003.

[12] J. H. McClellan and T. W. Parks, "Eigenvalues and Eigenvectors of the Discrete Fourier Transformation," *IEEE Trans. Audio and Electroacoustics*, Vol. 20, No. 1, March 1972.

[13] H. M. Ozatkas, O. Arikan, M. A. Kutay, G. Bozdagi, ”Digital Computation of the Fractional Fourier Transformation,” *IEEE Trans. Sig. Process.*, Vol. 44, No. 9, pp. 2141-2150, 1996.

[14] F. A. Grunbaum, ”The Eigenvectors of the Discrete Fourier Transform,” *Jour. Math. Analy.* & *Appl.*, Vol. 88, No. 2, pp. 355-363, 1982.

[15] X. -Gen. Xia, ”Discrete Chirp Fourier Transform and Its Application to Chirp Estimation,” *IEEE Trans. Sig. Process.*, Vol. 48, No. 11, pp. 3122-3133, 2000.

[16] C. Candan, M. A. Kutay, H. M. Ozatkas, ”The Discrete Fractional Fourier Transform,” *IEEE Trans. Sig. Process.* , Vol. 48, No. 5, pp. 1329-1337, 2000.

[17] Juan G. Vargas-Rubio, ”The Grunbaum Matrix and the Discrete Fractional Fourier Transform,” *Progress Report*, Nov. 2002.

[18] T. S. Santhanam, P. S. Chandrasekaran, N. B. Menon, ”General Involutional Transformations and Representation of GL(n),” *Journal of Mathematical Physics*, Vol. 12, No. 3, 1971.

[19] J. G. Vargas-Rubio, ”The Centered Discrete Fractional Fourier Transform, properties, computation, and application to linear chirp signals,” Ph.D Dissertation, The University of New Mexico, 2004.

[20] G. H. Golub and C. V. F. Van Loan, “Matrix Computations,” Third Edition, John Hopkins University Press, Baltimore, 1996.

[21] M. S. Richman, T. W. Parks, and R. G. Shenoy, “Discrete–Time, Discrete–Frequency, Time–Frequency Analysis,” *IEEE Transactions on Signal Processing*, Vol. 46, No. 6, 1998.

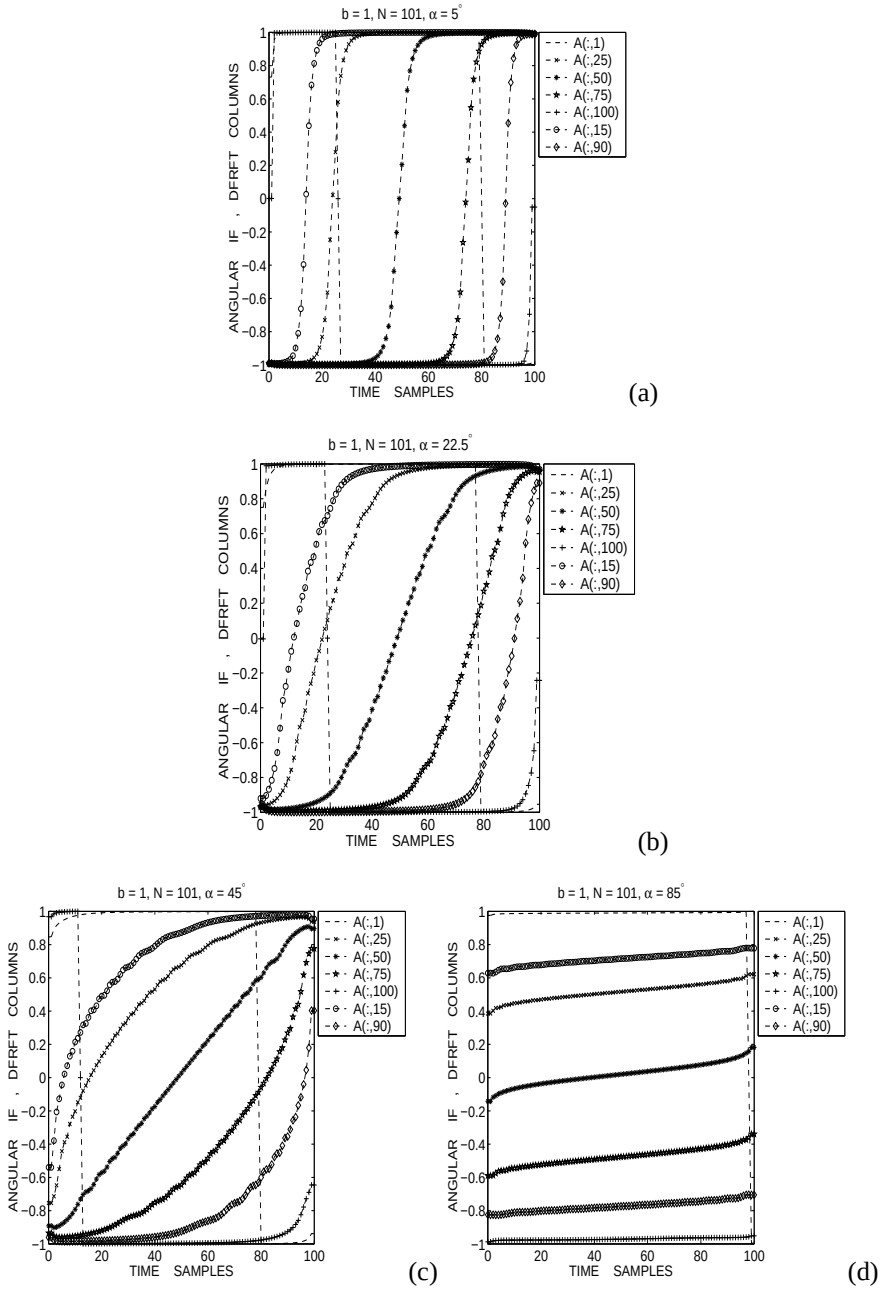

Figure 2: Normalized instantaneous frequency associated with different columns of the DFRFT operator for different angles. The IF of the DFRFT kernel is noticeably sigmoidal rather than linear.

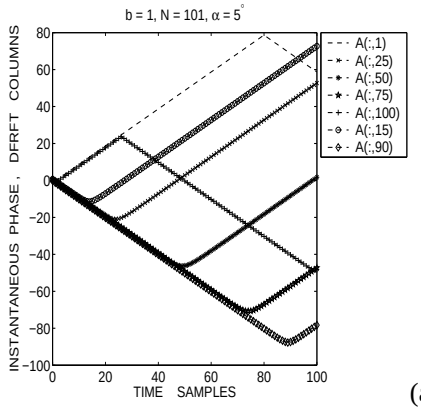

(a)

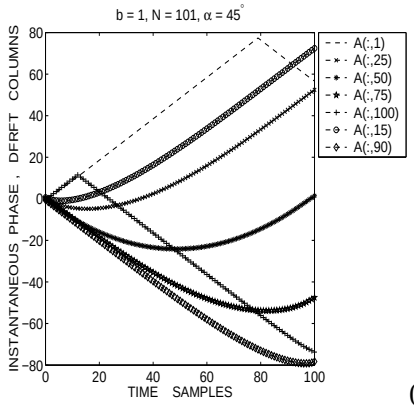

(b)

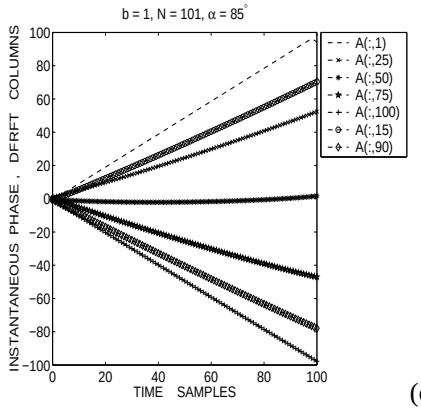

(c)

Figure 3: Normalized instantaneous unwrapped phase associated with the kernel of the DFRFT based on the Grunbaum commutor matrix.

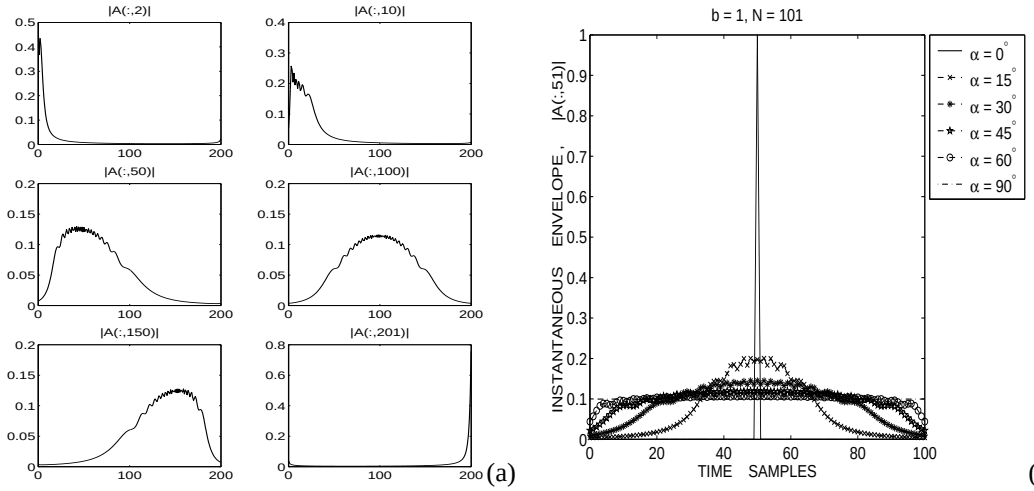

Figure 4: (a) Amplitude of different columns of the discrete FRET based on the Grunbaum commutor **T** for $N = 201, \alpha = 22.5^\circ, b = 1$, (b) instantaneous envelope of a fixed column for different angular parameters describing the increased spread of the envelope with increase in the angular parameter

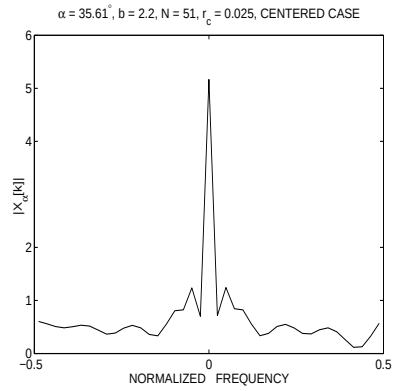

(a)

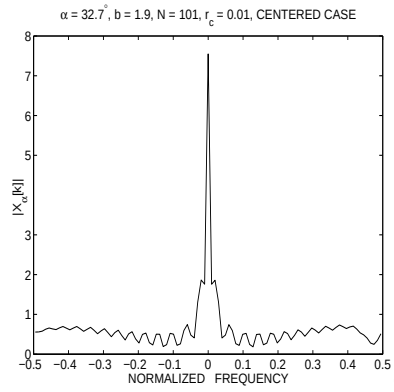

(b)

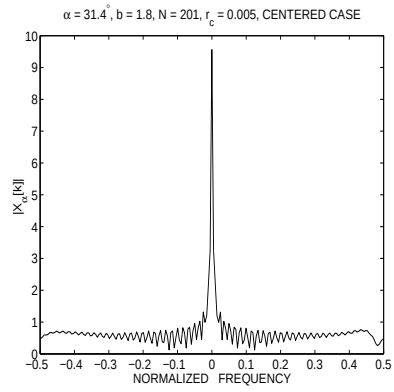

(c)

Figure 5: Magnitude of the DFRFT of chirp signals with different chirp rates $r_c = 0.005, 0.025, 0.01$ for specific angles and transform lengths N resulting in a impulse like transform.

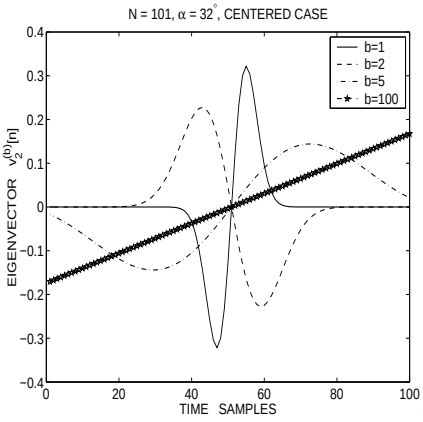

(a)

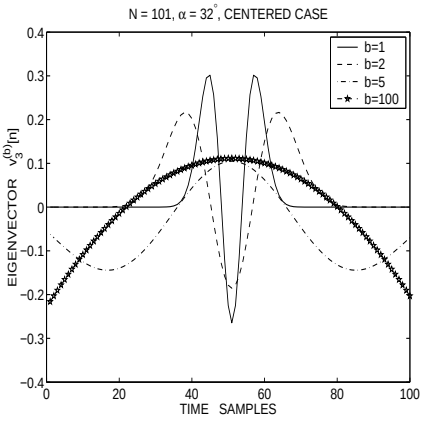

(b)

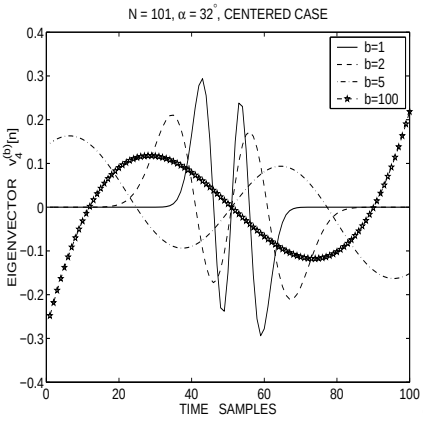

(c)

Figure 6: Eigenvectors $v_2[n]$, $v_3[n]$, $v_4[n]$ of the Grunbaum tridiagonal commuting matrix for $N = 201, \alpha = 22.5^\circ$ for different values of the dilation parameter.

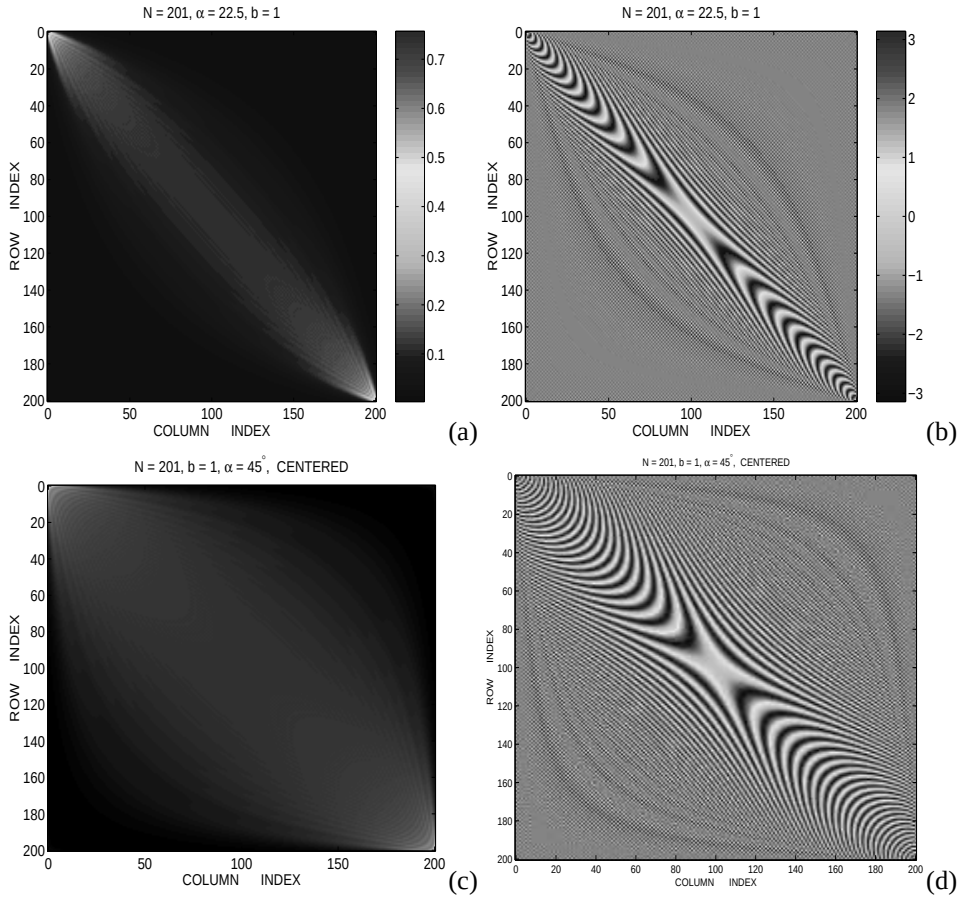

Figure 7: (a) Magnitude and (b) unwrapped phase of the elements of the DFRFT for $N = 201, \alpha = 22.5^\circ, b = 1$, (c) magnitude and (d) unwrapped phase of the elements of the DFRFT for $N = 201, \alpha = 45^\circ, b = 1$.

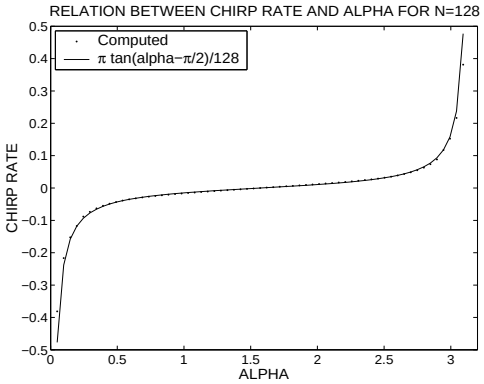

Figure 8: Relation between chirp rate and angle for $N = 128$. The solid line corresponds to the approximation in Eq. (16)

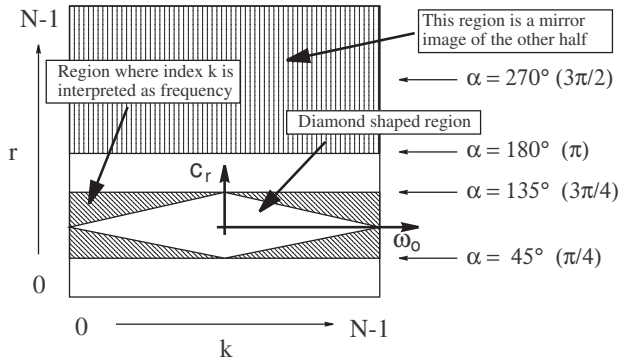

Figure 9: Map of $\mathbf{X}_k[r]$ that shows the region where the index k is interpreted as frequency.

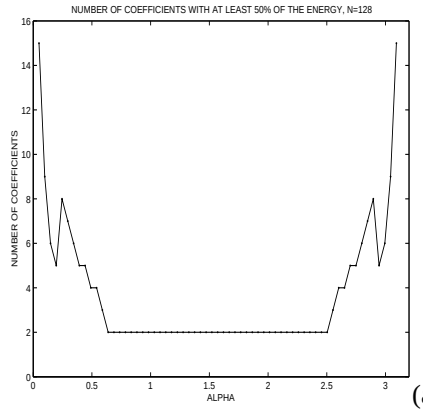

(a)

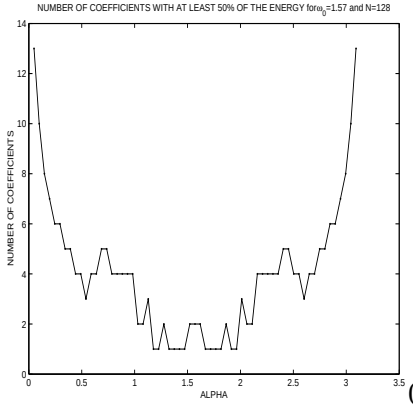

(b)

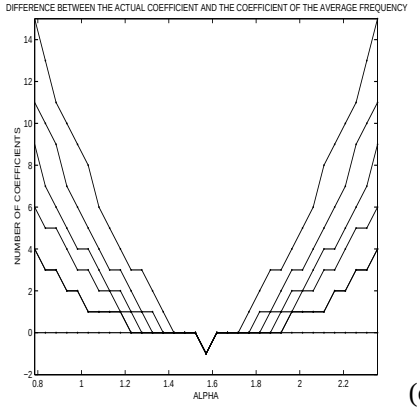

(c)

Figure 10: (a) Number of coefficients capturing 50% of chirp signal energy as a function of α with $w_0 = 0$, (b) with $w_0 = 1.57$, (c) number of coefficients of error in the localization of the average frequency with respect to α.

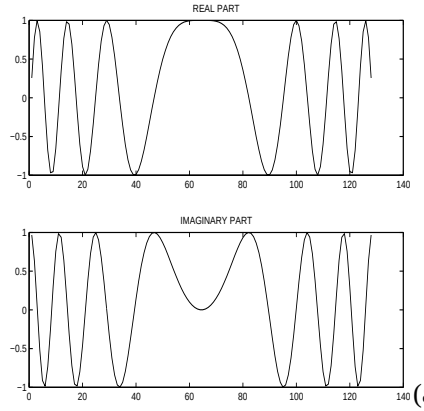

(a)

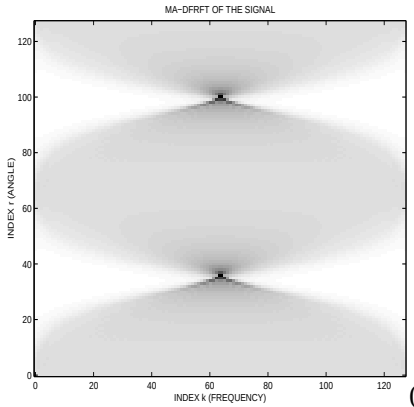

(b)

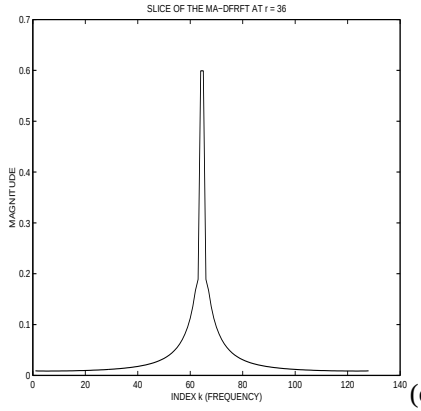

(c)

Figure 11: Monocomponent chirp: (a) chirp signal with a chirp rate, (b) magnitude of the corresponding MA-DFRFT, and (c) slices of the MA-DFRFT at $r = 36$.

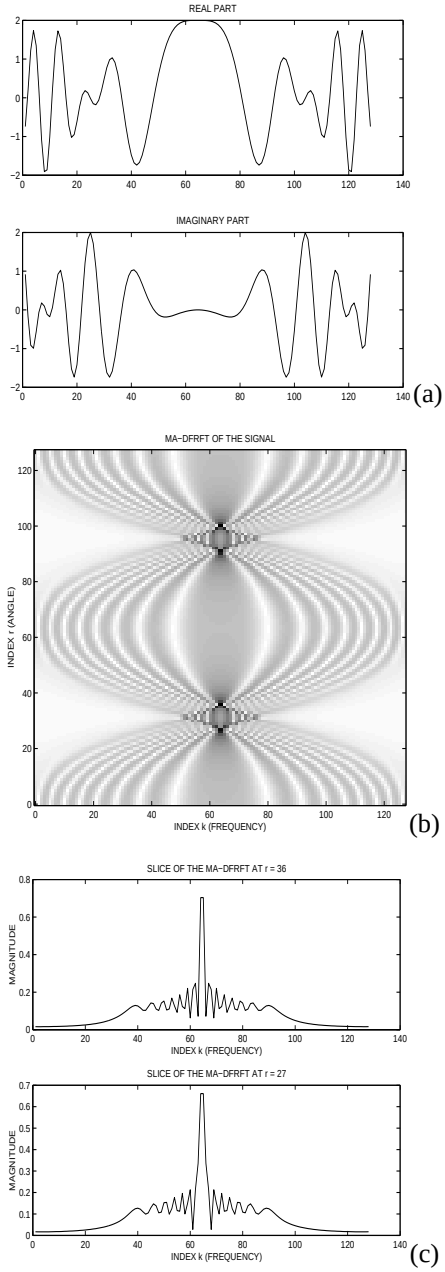

Figure 12: Two component chirp: (a) composite signal, (b) magnitude of the corresponding MA-DFRFT, and (c) slices of the MA-DFRFT at $r = 36$ and $r = 27$.